Sensors and Materials, Vol. 36, No. 10 (2024) 4165–4178
MYU Tokyo

S & M 3792

Analysis of Composition Formulas for Face-centered Cubic Solid Solution Alloys via Nearest-neighbor Two-shell Structure with Cowley Parameters

Hai-Lian Hong, Chi-Hsin Yang,* Hui-Xian Yan, and Ying-Yan Lin

School of Mechanical and Electric Engineering, Sanming University, Sanming 365004, Fujian Province, China

(Received April 30, 2024; accepted September 19, 2024)

Keywords: face-centered cubic (FCC), solid solution alloys, short-range order (SRO), solvated solute cluster (SSC), Friedel spherical periodic oscillation (FSPO)

The macroscopic properties of alloys are determined by their microstructure formed during solidification. In this study, we used the Friedel spherical periodic oscillation of electron density to characterize the nanoscale microstructure and accurately calculate the composition formula for the face-centered cubic alloy as $[A–B_{12}]C_3$ using Cowley parameters. Our analysis of various binary alloys shows that the obtained composition formulas align with those observed in grade alloys. This method holds promise for optimizing properties across diverse alloy systems.

1. Introduction

The determination of composition ranges for industrial alloys is primarily accomplished through extensive empirical experimentation, necessitating substantial human and material resources. To streamline the alloy development process, researchers have long been exploring the interrelationship among composition, microstructure, and alloy properties. X-ray spectroscopy, in conjunction with Fourier transform technology, is utilized for the analysis of internal atomic local structures in substances.[1] Neutron diffraction techniques are employed to examine the magnetic domain structure and thermal stress of materials,[2] while transmission electron microscopy (TEM) and scanning electron microscopy (SEM) are used to observe the precipitated phase and element distribution in alloys.[3]

The exceptional properties of alloys are derived from their stable microstructure, often characterized by the face-centered cubic (FCC) lattice structure at elevated temperatures,[4–8] which represents the thermodynamically favored phase for numerous industrial alloys. The stability of an alloy is primarily dictated by the atomic interactions within this stable phase. However, accurately determining the atomic cluster structure information of the high-temperature stable phase for multicomponent alloys under current experimental conditions remains a significant challenge. This limitation impedes the study of alloy properties from an analytical chemical composition perspective and hinders rational knowledge of alloy

*Corresponding author: e-mail: 20190207@fjsmu.edu.cn
https://doi.org/10.18494/SAM5100

ISSN 0914-4935
https://myukk.org/

composition design and modification. Therefore, modeling the chemical structure of solid solution alloys serves as a universal foundation for alloy composition design.

The majority of alloys utilized in industrial applications are predominantly based on the austenite γ phase,[9–11] with secondary phase particles dispersed using various processing techniques to enhance the irregularity and atomic energy within the atomic arrangement of an alloy. This serves to impede dislocation movement within the alloy, thereby increasing its strength while also improving its toughness and plasticity.[9,10] In single-phase solid solution alloys, the internal stress field is generated by lattice distortion resulting from atomic size mismatch, thereby hindering dislocation glide and enhancing the mechanical properties of the alloys. However, despite maintaining the crystal structure of the solvent in the long range, the distribution of solute atoms in solid solutions is irregular.[11] Understanding the distribution of solute atoms and their interaction mechanism with solvent atoms is crucial for establishing a comprehensive chemical structure model of solid solutions.

The macroscopic properties of a material are primarily dictated by the atomic interactions within its microstructure. These interactions, particularly those occurring between nearest-neighbor atoms, play a pivotal role in shaping the material's behavior. Extensive research has shown that short-range order in FCC solid solution alloys exerts marked effects on deformation microstructure and associated mechanical behavior.[12,13] On the basis of the classical solid solution theory, the nearest-neighbor atomic interaction model suggests that in a binary solid solution, when the exchange energy W of the nearest-neighbor atoms is less than 0 ($W < 0$), the segregation of similar atoms occurs. Conversely, when $W > 0$, the segregation of unlike atoms is observed. This implies that there will be numerous clusters of short-range-ordered (SRO) structures present in the alloys,[14] such as solute and solvent clusters, and solvated solute clusters (SSCs) as depicted in Fig. 1.

The clusters exhibit specific magic number characteristics[15–18] and relatively stable atomic structures. The highest stability among the three types of cluster is observed only in SSCs, attributed to the difference in electronegativity between solvent and solute atoms. Researchers

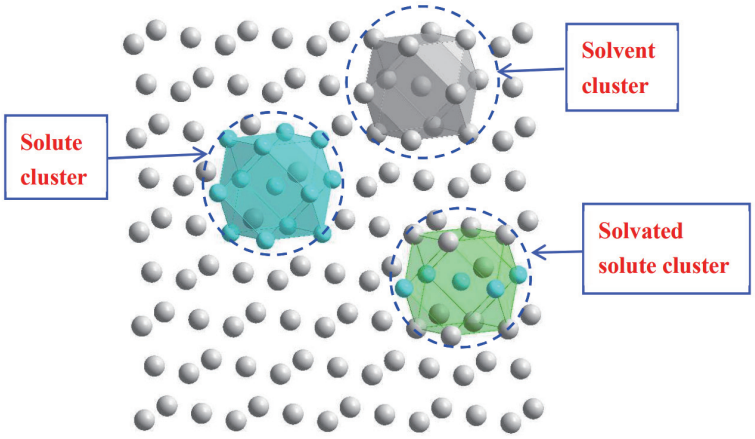

Fig. 1. (Color online) Three types of cluster in alloys.

discovered a high abundance of SSCs in the alloys, with their number density and volume fraction surpassing those of the precipitated phase.[19–23] In single-phase solid solutions, solute atoms typically exist in the substrate as a solid solution. The increase in alloy strength primarily stems from lattice volume mismatch and the pinning of elastic mismatch dislocations caused by solid solution atoms, known as solid-solution strengthening.[21] In the context of an alloy containing a precipitated phase, the precipitated phase particles act as pinning sites, impeding dislocation movement. However, nano-precipitated phase particles with a crystalline structure exhibit strong interaction with the substrate, leading to significant stress and strain concentration around the precipitated phase. When there is a deformation imbalance between the precipitated phase and the substrate, micropores are formed and crack propagation is accelerated, ultimately reducing the ductility and fracture toughness of the alloy.[22–24]

The SSC characterized by a size intermediate between that of the solute atom and the precipitated phase exhibits a dislocation-hindering effect that exceeds that of a single atom but falls short of the impact of the precipitated phase. However, owing to its ability to achieve a high density with a number density that is an order of magnitude higher than that of the precipitated phase, its strengthening effect is significantly amplified. At the same time, it causes notably less damage to the plastic toughness of the alloys compared with the precipitated phase.[25] Nevertheless, establishing a strengthening model for SSCs poses significant challenges owing to their nonuniform chemical composition and disordered structure.

Zhang *et al.*[26] and Li *et al.*[27] utilized the cluster-plus-glue-atoms model to elucidate the ordered structure of adjacent two-shell atoms in an alloy and subsequently applied their findings to analyze the chemical composition formula of FCC solid solution alloys. Although the alloy composition derived from this model generally aligns with expected alloy-grade compositions, further validation is essential to confirm the accuracy of this cluster-plus-glue-atoms model in analyzing the chemical composition of FCC solid solution alloys owing to specific issues.

First, the chemical composition formula of the first nearest-neighbor shell atoms in the obtained chemical formula is rounded to facilitate practical analysis and modeling. For example, on the basis of Cowley parameters, the number of Cu atoms in the first nearest-neighbor shell of the grade alloy $Cu_{68.9}Zn_{31.1}$ is approximated to 10. This rounding process simplifies and approximates complex atomic arrangements for practical analysis and modeling purposes, enhancing their feasibility for computational simulations and theoretical studies. Furthermore, the distribution of the second nearest-neighbor shell atoms in the obtained alloy chemical composition formula is determined through empirical equations utilizing atomic radius and the number of atoms in the amorphous alloy structure. The studies have concluded that the quantity of atoms within the elemental cluster is directly proportional to both the mean atomic density and the cubic value of the radius of the sphere surrounding the first nearest-neighbor shell polyhedron. However, owing to the lattice atom occupancy characteristics of FCC solid solutions, there exists a distinct relationship between atom density in the alloys and their volume occupied by atoms compared with amorphous alloys. Therefore, further analysis is required for the research conclusions obtained from Refs. 26 and 27.

From the preceding analysis, there is still potential to improve the accuracy of FCC solid solution alloy chemical composition analysis through the application of the cluster-plus-glue-

atoms model. This study's primary contribution lies in its investigation of FCC solid solution alloys. Initially, we utilized the spherical period oscillation mechanism to elucidate electron fluctuation behavior and determined the range of shielding solute impurities within FCC solid solution alloys. Subsequently, by comparing with the lattice position of FCC solid solutions, we identified the range of central atoms within two clusters in their nearest shell. Following this, we selected optimal models for the first and second nearest-neighbor shell structures in FCC solid solutions. Finally, atomic chemical composition formulas for subsequent neighboring shells in FCC solid solution alloys were calculated using Cowley parameters specific to these adjacent shells.

According to the analysis of the known Cowley parameters for grade alloys, it is evident that the chemical composition formula derived in this study closely aligns with the composition of the grade alloys. This alignment suggests that the chemical composition of an alley can be attributed to a stable nearest-neighbor two-shell atomic structure. The novelty of this study is that the presented findings lend support to the research approach and methodology for analyzing and comprehending alloying chemical compositions from a cluster structure perspective.

The subsequent sections of this study are organized as follows. In Sect. 2, the number of nearest-neighbor atomic shells is determined by analyzing the Friedel spherical periodic oscillation (FSPO) of electron density, along with a detailed presentation of the configuration and spatial arrangement of the atomic shells. In Sect. 3, we introduce and propose cluster models for FCC solid solution alloys, presenting positional vector sets for the nearest-neighbor atomic shells and identifying the most suitable cluster model, referred to as the 1-3 model. In Sect. 4, the composition formulas for several binary solid solution alloys are verified using Cowley parameters from previous works in conjunction with the proposed cluster model. Finally, conclusions are provided.

2. Determination of Number of Nearest-neighbor Atomic Shells

The analysis of the alloy composition formula solely relied on the SSC model with the first nearest-neighbor shell interaction, which failed to adequately elucidate the coexistence of ordering and spinodal decomposition.[28] Consequently, there is a significant discrepancy between the alloy properties calculated in Ref. 28 and the measured results.

The model proposed in Ref. 29 considers the interaction of the first and second nearest-neighbor shell atoms to analyze the alloy composition formula. This model effectively elucidates the coexistence of ordering and spinodal decomposition. Moreover, the calculated results derived from this model, such as misalignment energy, magnetic susceptibility, ordering temperature, and the frequency of the crystal lattice wave, are in line with experimental findings.[29,30] When investigating the properties of alloys, especially long-range disordered solid solution alloys, it is crucial to analyze the atomic structure of the second nearest-neighbor shell. This is due to the weak Coulomb interaction between electrons and atoms, which predominantly affects the nearest- and next-nearest-neighbor shell atoms. Understanding this arrangement is essential for comprehending the material's behavior.

Häussler[31] presented a rigorous computational approach for the model postulated in Ref. 29. In solid solution alloys, the ingress of impurities (solute atoms) into the solvent atom substrate

induces the polarization of the electron cloud surrounding the impurity charge, resulting in an incomplete shielding effect on the overall system perturbation. The participating electrons primarily reside on the Fermi surface.[31] Owing to the diffraction effects of De Broglie material waves from these electrons interacting with impurities, an oscillatory charge distribution emerges around them, known as FSPO.[31] The origin of this oscillation can be attributed to discontinuous changes in occupied states on the Fermi surface. Consequently, electron interaction is no longer simply governed by the Coulomb potential, but rather by an effective pair potential in FSPO. The effective pair potential $\varphi(r)$ for the electrons is formed by $\varphi(r) \propto \cos(2\vec{k}_F \cdot \vec{r} + \theta) / r^3$, where $\vec{k}_F$ represents the Fermi vector, $\vec{r}$ is the radial position vector to solute atoms, and θ denotes the phase shift angle.

The momentum exchange between electrons and atoms results in the resonance of the scattered wave and the distributed wave of the atom, induced by electron oscillation. This process leads to the formation of a pseudo-gap at the Fermi energy level, thereby lowering the band structure energy $\Phi_{band\_str.}$ of the entire system. Consequently, atoms are positioned within the lowest energy gap, rendering the alloy structure more stable. The band structure energy $\Phi_{band\_str.}$ is defined by

$$\Phi_{band\_str.} = \alpha \int [p(r) - 1] \varphi(r) r^2 dr, \tag{1}$$

where $p(r)$ is the particle density function at the distance r and α is a proportionality constant. When the maximum value of the particle density function $p(r)$ corresponds to the minimum value of the effective pair potential function $\varphi(r)$, resulting in a minimized $\Phi_{band\_str.}$ and the lowest overall energy for the atomic system, a state of heightened stability is formed. Figure 2 shows the position of the troughs on $\varphi(r)$ located at distances $r_n = (1/4 + n)\lambda_{Fr}$, $n = 1, 2, 3, \ldots$ from the central atom, where λ_{Fr} represents the Friedel wavelength and n denotes the n-th atomic shell. When the effective pair potential function $\varphi(r)$ demonstrates the periodic and oscillatory convergent distribution, FSPO is considered to emerge.

In this study, we performed an in-depth analysis of the composition formula of FCC solid solution alloys, offering a novel insight into the morphological characteristics of individual atomic shells within the FCC solid solution alloys. Furthermore, we defined their precise positions within FSPO. Figure 2 shows the configuration and spatial arrangement of the first to ninth atomic shells, as well as the 13th shell, with respect to the central atom at origin O. The ordinate axis represents the effective pair of the potential function $\varphi(r)$ of the FSPO, while the abscissa axis denotes the position r of each atomic shell from origin O.

As illustrated in Fig. 2, at $r_5 = 5.25\lambda_{Fr}$, the oscillatory pattern of the effective pair potential function $\varphi(r)$ becomes less discernible and tends to be flat, indicating that the atoms in this region are approaching a state of reduced perturbation by the central solute atom. In fact, beyond the midpoint between r_4 and r_5, the region is electrically neutral, effectively shielding impurity charge oscillations. This position is formally defined as the truncation radius r_{cut}, calculated as $(r_4 + r_5)/2 = 4.75\lambda_{Fr}$. The 13th shell atom of the FCC solid solution resides at $r = 4.51\lambda_{Fr}$, whereas the 14th shell atom is positioned at $r = 4.84\lambda_{Fr}$. Consequently, only 13 atomic shells exist within the truncation range of FSPO.

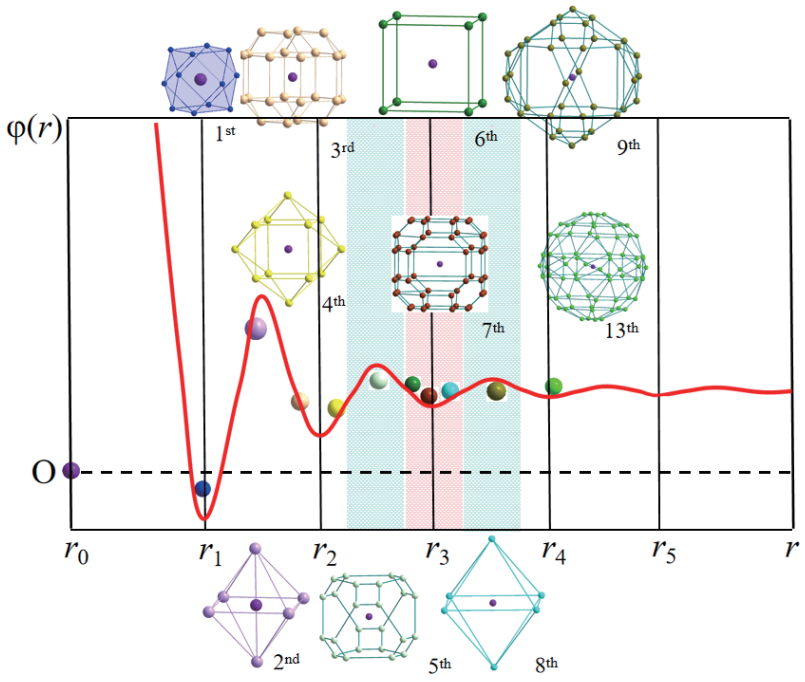

Fig. 2. (Color online) Positions of atomic shells in FSPO.

3. Cluster Models of FCC Solid Solution Alloys

If it is located at origin O, a cluster Ω is designated as the central cluster. As depicted in Fig. 2, the stable position for the other independent cluster, which is referred to as cluster Π, should be within the troughs of r_1, r_2, r_3, and r_4. Given that position r_1 represents the shell atomic location of cluster Ω, no other clusters can coexist at this specific site. The reason is described as follows. If cluster Π was to occupy position r_2, there would be an interaction and sharing of shell atoms between clusters Π and Ω leading to a disruption of their composition and structure. Consequently, it is precluding the existence of two independent clusters. Therefore, the most stable position for the nearest-neighbor cluster Π closest to the central cluster Ω is at r_3. Cluster Π, with the seventh shell atom as its core atom, demonstrates the closest spatial proximity and the highest thermodynamic stability to cluster Ω, thereby classifying it as the nearest-neighbor cluster.[32]

Hong *et al.* documented a comprehensive analysis of all models in FCC solid solution alloys, comparing these models with the positions of the nearest-neighbor clusters.[32] The most suitable model for the shell position structure of FCC solid solution alloy clusters that satisfies FSPO can be obtained. For ease of analysis and comparison, the vector sets of the shell atoms of clusters in FCC solid solution alloys are defined below.

The defined coordinate system has its origin at atom O, with coordinates O(0, 0, 0) as illustrated in Fig. 3. At this position, there exists a central cluster Ω. From the shape and position of the atomic shell depicted in Fig. 2, there are 12 atoms on the first shell of cluster Ω representing the first nearest-neighbor shells of atom O as P_1 to P_{12}. P_7 is positioned at the center of the

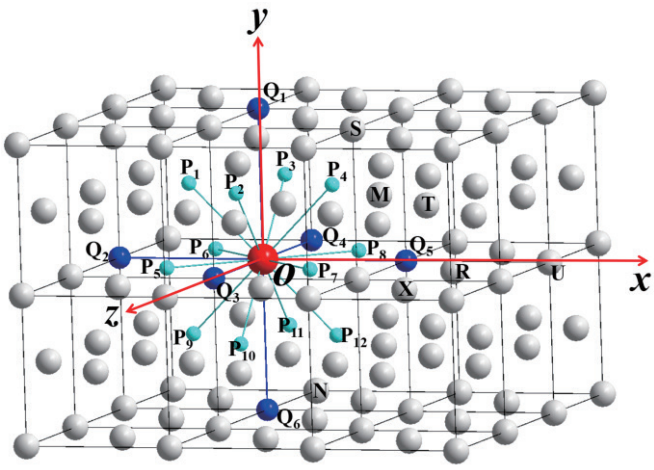

Fig. 3. (Color online) Atomic occupancy of FCC alloys.

surface with coordinates (1/2, 0, −1/2), and its position vector should be [1/2, 0, −1/2] if the lattice constant is assumed to be 1. The position coordinates for the remaining 11 atoms are listed in Table 1. The set of position vectors for P_1 to P_{12} follows the solid-state physics equivalent crystal direction expression method,[33] defined as P < ±1/2, ±1/2, 0 >.

Similarly, six atoms form the second nearest-neighbor shell with atom O from Q_1 to Q_6; their position coordinates and vector sets are also listed in Table 1. Assuming that a prion called M lies in the third nearest-neighbor shell with coordinates (1, 1/2, 1/2) and another called N lies in the fourth nearest-neighbor shell with coordinates (0, −1, −1), their corresponding sets of position vectors are M < ±1, ±1/2, ±1/2 > and N < ±1, ±1, 0 >.

The coordination of representative atoms in the 5th to 9th atomic shells from the central atom O is as follows: R(3/2, 0, 1/2), S(1, 1, 1), T(3/2, 1/2, 1), U(2, 0, 0), and X(3/2, 0, 3/2). The vector sets corresponding to these atomic shells are also detailed in Table 2. To determine the position of the nearest-neighbor cluster model within the atomic shell that may generate FSPO in the FCC solid solution, we analyzed the 18 potential cluster models of the FCC solid solution based on Ref. 32 in this study. Six suitable candidate cluster models are presented in Table 3. Moreover, each individual atomic shell is conceptualized as a sphere with varying radius. The spatial arrangement of additional clusters centered on cluster Ω within the same sphere and the number of clusters present at this specific location are also shown in Table 2 for each potential FCC cluster model.

From the 18 potential cluster models of the FCC solid solution proposed by Hong *et al.*,[32] note that clusters can potentially exist from the 5th atomic shell to the 11th atomic shell. However, owing to specific constraints and considerations, it has been noted that the locations of clusters surrounding the centered cluster Ω are restricted to shells 5 to 9.

1. When the cluster is located at the 10th atomic shell and beyond, the interatomic distances within the shell exceed the truncation radius r_{cut} of FSPO, leading to the positional instability of its constituent atoms.
2. Positioned at the fourth atomic shell < ±1, ±1, 0 >, the cluster shares this location with the central cluster Ω as depicted in Fig. 4(a). As it approaches closer to the central cluster Ω, for

Table 1
Coordinates of atoms and vector sets of the first and second shells.

	First shell		Second shell
Coordinates of atoms	$P_1(-1/2, 1/2, 0)$	$P_2(0, 1/2, 1/2)$	$Q_1(0, 1, 0)$
	$P_3(0, 1/2, -1/2)$	$P_4(1/2, 1/2, 0)$	$Q_2(-1, 0, 0)$
	$P_5(-1/2, 0, 1/2)$	$P_6(-1/2, 0, -1/2)$	$Q_3(0, 0, 1)$
	$P_7(1/2, 0, 1/2)$	$P_8(1/2, 0, -1/2)$	$Q_4(0, 0, -1)$
	$P_9(-1/2, -1/2, 0)$	$P_{10}(0, -1/2, 1/2)$	$Q_5(1, 0, 0)$
	$P_{11}(0, -1/2, -1/2)$	$P_{12}(1/2, -1/2, 0)$	$Q_6(0, -1, 0)$
Vector set	$P < \pm 1/2, \pm 1/2, 0 >$		$Q < \pm 1, 0, 0 >$

Table 2
(Color online) Comparison of FCC alloy cluster locations with FSPO locations.

Shell No.	Vector set	Model					
		1-1	1-2	1-3	1-4	1-5	1-6
5	$R < \pm 3/2, \pm 1/2, 0 >$	6	6	—	4	4	—
6	$S < \pm 1, \pm 1, \pm 1 >$	—	—	8	—	—	2
7	$T < \pm 3/2, \pm 1, \pm 1/2 >$	6	2	—	4	—	6
8	$U < \pm 2, 0, 0 >$	—	—	6	—	2	—
9	$X < \pm 3/2, \pm 3/2, 0 >$	—	2	—	2	6	6
(Average distance of atoms with respect to center)/λ_{Fr}		3.052	3.090	3.266	3.192	3.397	3.463
Deviation of mean distance with respect to r_3 (%)		6.1	4.9	**0.5**	1.8	4.5	6.6
Coordination number		12	10	14	10	12	14

'—' denotes the non-existence of clusters within the corresponding shell in Table 2.

Table 3
(Color online) Atomic arrangements of candidate cluster models.[32]

Model No.	1-1	1-2	1-3
Cluster arrangement	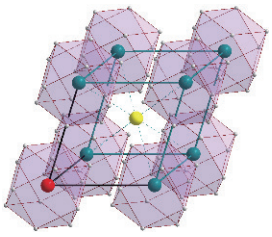	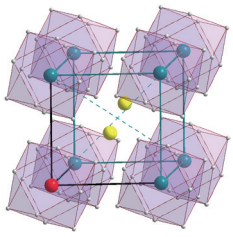	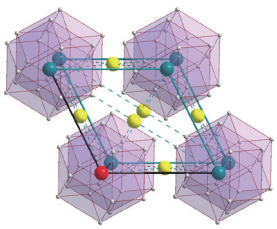
Model No.	1-4	1-5	1-6
Cluster arrangement	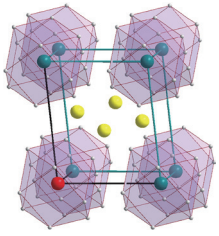	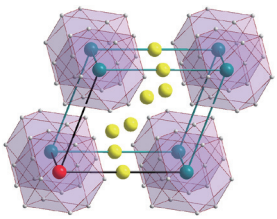	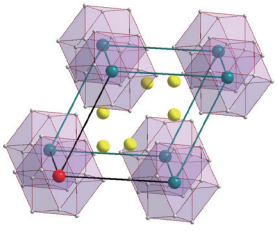

example, at a position such as the third atomic shell $< \pm 1, \pm 1/2, \pm 1/2 >$ shown in Fig. 4(b), an increased number of shared atoms between them results in the disruption of their composition and structure.

Hence, the nearest-neighbor clusters satisfying FSPO are expected to be positioned within the 5th to 9th shell atoms, with corresponding vector sets including $< \pm 3/2, \pm 1/2, 0 >$, $< \pm 1, \pm 1, \pm 1 >$, $< \pm 3/2, \pm 1, \pm 1/2 >$, $< \pm 2, 0, 0 >$, and $< \pm 3/2, \pm 3/2, 0 >$, respectively.

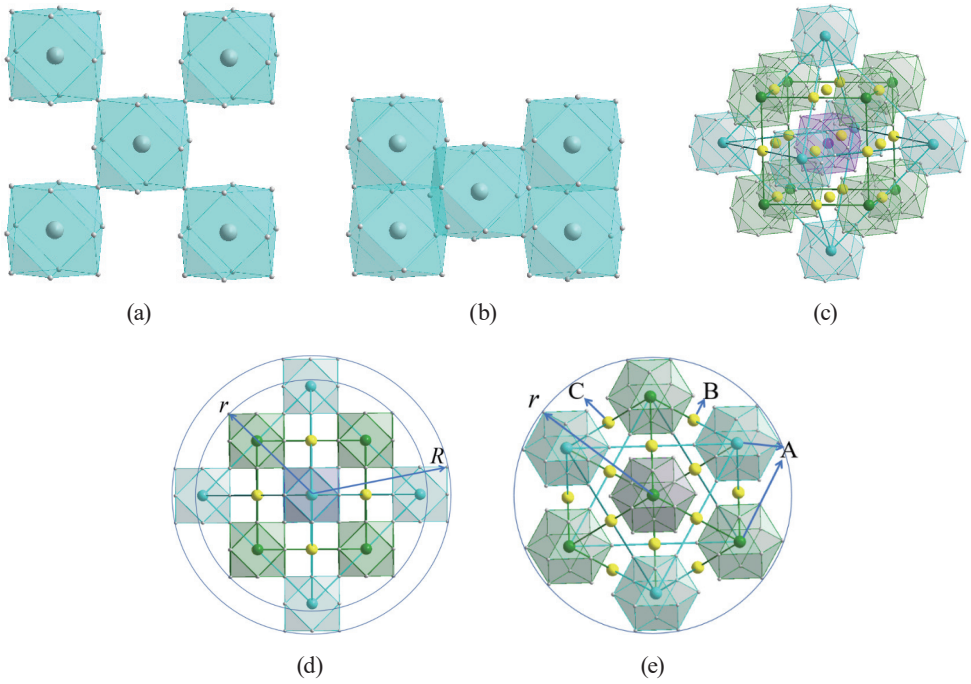

Fig. 4. (Color online) Arrangement and symmetry of the 1-3 model. (a) Two adjacent clusters share one shell atom, (b) two adjacent clusters share four shell atoms, (c) outside coordination of central cluster, (d) fourth symmetry, and (e) hexagonal symmetry.

In Fig. 2, we examine the region of trough (the pink region) at the position r_3 in the effective pair potential function $\varphi(r)$, where the left and right distances constitute the width range of $\lambda_{Fr}/2$. There are only three cases of vector sets for the nearest-neighbor cluster falling within this region, namely, the sixth atomic shell < ±1, ±1, ±1 >, the seventh atomic shell < ±3/2, ±1, ±1/2 >, and the eighth atomic shell < ±2, 0, 0 >. Consequently, it can be inferred from Table 2 that the most suitable cluster model satisfying FSPO is confined to the 1-3 model. The rationale for this analysis is detailed below.

1. As per the findings from Fig. 2 and Table 2, it is evident that the first and second atomic shells in the 1-3 cluster model are positioned within the trough at r_3. The average distance of all 14 cluster atoms in these two shells relative to the central cluster Ω measures at $3.266\lambda_{Fr}$, demonstrating a minimal variance from $r_3 = 3.25\lambda_{Fr}$.
2. In accordance with the principle of minimum energy, a more compact arrangement of clusters leads to a lower Coulomb potential energy owing to the closer proximity of atoms to the shared electron cloud, resulting in the increased stability of cluster binding. Table 2 reveals that the 1-3 cluster model exhibits a coordination number of 14,[32] indicating its highly dense packing as depicted in Fig. 4(c).
3. The 1-3 cluster model demonstrates the most homogeneous distribution of shells, resulting in the minimal deviation percentage ratio relative to $r_3 = 3.25\lambda_{Fr}$ for the average distance of all atoms from the central cluster. Within this model, only two shell clusters are positioned at a distance of r_3 around the central cluster Ω. When considering the cluster as a unit, it becomes apparent that the cluster with a vector set < +1, +1, +1 > containing eight atoms in the eighth nearest-neighbor shell is one atom closer than r_3, whereas the cluster with a vector set < ±2, 0,

0 > containing six atoms in the sixth nearest-neighbor shell is one atom farther than r_3. This configuration represents an optimal structure for clusters to satisfy both planar and spherical periodic orders.

4. Using an aluminum-based alloy as a case study, with a lattice constant of α = 0.405 nm and 428 atoms within the FSPO range, we estimated the size of FSPO as 2.3 nm on the basis of the position of the 15th atomic shell. According to the 1-3 model depicted in Fig. 4(d), an atom situated at distance R from the central cluster Ω is positioned in the 13th atomic shell, characterized by a vector set of < ±1/2, 0, ±5/2 >. The SSC is estimated to be 2.1 nm in size. Similarly, an atom located at distance r from the central cluster Ω resides in the 11th atomic shell with a vector set of < ±3/2, ±3/2, ±1 >, and its corresponding SSC has an estimated size of 1.9 nm. Sun *et al.*[19] and Zhang *et al.*[34] suggested that for aluminum-based alloys, the SSCs should not exceed sizes of up to 2 nm. However, their failure to consider 16 outermost atoms may lead to deviations in these estimations. Conversely, Song *et al.*[35] argued that sizes can range between 1 and 3 nm, further supporting our selection for truncation radius within FSPO.
5. On the basis of the 1-3 model, it is observed that FCC solid solution alloys exhibit a high degree of symmetry in their cluster arrangement. As depicted in Fig. 4(d), the alloys' clusters demonstrate quadratic axisymmetric properties, whereas Fig. 4(e) illustrates hexagonal axisymmetric properties. The higher the symmetry of the cluster arrangement, the more symmetrical the distribution of electron pairs around the central cluster at maximum angle, resulting in larger bond angles between shared electrons and reduced electric repulsion forces. This leads to a more stable overall alloy structure due to minimized steric hindrance and enhanced electronic delocalization within the alloy clusters.

The stable cluster arrangement structure in the alloy can be likened to the molecular formula of a compound, resulting in a corresponding chemical composition formula. It reflects the spatial configuration and stoichiometry of atomic clusters within the alloy. In the FCC solid solution alloy, the chemical composition formula for the 1-3 model is denoted as $[A–B_{12}]C_3$. Here, A represents the central atom of the cluster, as depicted in Fig. 4(c) showing all truncated octahedrons, whereas B signifies the shell atom of the cluster, i.e., the first neighbor atoms surrounding the central atom A with a quantity of 12, as shown in Fig. 4(c) for all shell atoms of the truncated octahedron. C denotes the second nearest-neighbor atom surrounding the central atom A with a quantity of 3, represented by all yellow atoms shown in Fig. 4(e).

One cluster with three second nearest-neighbor atoms forms a cluster cell unit. The formation of a nanoscale SSC is facilitated by stacking the cluster cell unit to the size of the truncation radius determined by FSPO. The abundance of SSCs with the SRO structure in FCC solid solution alloys has been demonstrated in multiple experimental studies, which show an increase in local lattice distortion energy attributable to atoms with large size mismatches. This promotes the rearrangement of local atoms with high chemical affinity and results in the formation of relatively strong chemical bonds between atoms. The SRO structure of SSCs interacts with dislocations to enhance the mechanical properties of an alloy, improving both strength and plasticity simultaneously.

4. Analysis of Cowley Parameters of FCC Solid Solution Alloy Model

To quantitatively comprehend the SRO distribution of solute atoms in binary solid solutions, we utilize the SRO Cowley parameter $\gamma = 1 - P_A/X_A$ to represent this arrangement.[36] Here, P_A denotes the probability of atom A surrounding atom B, and X_A represents the mole fraction of atom A. When A and B atoms are disordered, $\gamma < 0$. When they are evenly distributed, $\gamma > 0$. The values of SRO Cowley parameters can be determined through experimental measurements or computer simulations. These parameters result from a large number of statistical averages, effectively addressing the issue of atom occupation on different shells in solid solution alloys.[36–39]

In the analysis of Ni alloy, Schönfeld *et al.*[37] conducted elastic neutron scattering experiments on three samples of Ni–20 at% Cr alloy with initial concentrations placed at different temperatures and aging times: 741 K for 480 h, 828 K for 320 h, and 937 K for 2.6 h. The actual concentrations of the samples were determined to be Sample 1: Ni–21.3 at% Cr, Sample 2: Ni–20.1 at% Cr, and Sample 3: Ni–20.6 at% Cr using X-ray fluorescence analysis, where at% represents the atomic percentage of Ni in the alloy. Subsequently, the SRO Cowley parameters of the three samples were obtained through a least-squares fitting procedure.[37] This allowed for a comprehensive understanding of the microstructural evolution and phase transformations in these alloys under different thermal conditions.

The Cowley parameters for the nearest-neighbor two-shell atoms in Sample 1 are $\alpha_{110} = -0.1061$ and $\alpha_{200} = 0.0891$. According to the Cowley formula, the atomic arrangement of the nearest-neighbor two-shell atoms centered on Ni can be calculated as $[Ni–Ni_{9.17}Cr_{2.83}]Ni_{2.42}Cr_{0.58}$. When there are three atoms in the second shell, the chemical composition of the alloy is determined to be 21.31%, which closely aligns with the actual alloy composition with a deviation of only −0.04%. This indicates that employing the nearest-neighbor two-shell atomic model enables the precise resolution of the composition formula for binary solid solution alloys.

The research methodology proposed by Schönfeld *et al.*[37] can be corroborated in other alloys. Table 4 shows the Cowley parameters of several binary solid solution alloys and the at% values of component A in the composition formula. It is evident from the relative deviation in Table 4 that the compositions of these chemical composition formulas, calculated using the first and second nearest-neighbor Cowley parameters, are generally congruent with that of the alloy. Only a few alloys exhibit slightly larger composition deviations, which may be attributed to excessive lattice defects within the alloys' internal structure and suboptimal atom distribution during sample preparation processes.

The composition formula corresponding to the 1-3 model, $[A–B_{12}]C_3$, delineates the average cluster structure of the nearest-neighbor shell atomic distribution. From the experimental statistical averages of Cowley parameters, SRO structures are highly probable. However, various factors such as the collision of adjacent grains during crystal growth or thermal stress from volume changes during cooling can lead to vacancies and dislocations in the crystal lattice, causing abrupt changes in atomic arrangement. To enhance the properties of an alloy for practical applications, additional trace elements are incorporated into the alloy.

For instance, a small amount of carbon atoms may be added to improve resistance to electrochemical corrosion by occupying interstitial sites within the crystal lattice. This further

Table 4
Cluster composition formulas of FCC solid solution alloys.

Alloy	Component of A (at%)	Cowley parameters (γ)	Composition formula	Component of A in formula (at%)	Deviation (%)
CrNi[37]	21.3	$\alpha_{110} = -0.1061$ $\alpha_{200} = 0.0891$	$[Ni–Ni_{9.17}Cr_{2.83}]Ni_{2.42}Cr_{0.58}$	21.31	−0.0004
CrNi[37]	20.1	$\alpha_{110} = -0.099$ $\alpha_{200} = 0.849$	$[Ni–Ni_{9.35}Cr_{2.65}]Ni_{2.91}Cr_{0.09}$	17.14	0.1474
CrNi[37]	20.6	$\alpha_{110} = -0.0819$ $\alpha_{200} = 0.0635$	$[Ni–Ni_{9.33}Cr_{2.67}]Ni_{2.42}Cr_{0.58}$	20.33	0.0130
FeNi[38]	50	$\alpha_{110} = -0.13$ $\alpha_{200} = 0.17$	$Ni–Ni_{5.22}Fe_{6.78}–Ni_{1.76}Fe_{1.24}$	50.16	−0.0031
WNi[38]	13	$\alpha_{110} = -0.19$ $\alpha_{200} = 0.23$	$Ni–Ni_{10.14}W_{1.86}–Ni_{2.7}W_{0.3}$	13.48	−0.0369
AuCu[38]	25	$\alpha_{110} = -0.195$ $\alpha_{200} = 0.215$	$[Cu–Cu_{8.41}Au_{3.59}]Cu_{2.41}Au_{0.18}$	26.09	−0.0434
AuCu[38]	50	$\alpha_{110} = -0.123$ $\alpha_{200} = 0.048$	$[Cu–Cu_{5.26}Au_{6.74}]Cu_{1.57}Au_{1.43}$	51.04	−0.0208
AuCu[38]	75	$\alpha_{110} = -0.08$ $\alpha_{200} = 0.19$	$[Cu–Cu_{2.28}Au_{9.72}]Cu_{1.82}Au_{1.18}$	72.14	0.0381
AlCu[38]	14.5	$\alpha_{110} = -0.14$ $\alpha_{200} = 0.12$	$[Cu–Cu_{10.02}Al_{1.98}]Cu_{2.62}Al_{0.38}$	14.79	−0.0200
FePd[38]	25	$\alpha_{110} = -0.14$ $\alpha_{200} = 0.28$	$Fe–Fe_{8.58}Pd_{3.42}–Fe_{2.46}Pd_{0.54}$	24.75	0.01
AuAg[38]	50	$\alpha_{110} = -0.08$ $\alpha_{200} = 0.01$	$[Ag–Au_{6.48}Ag_{5.52}]Au_{1.49}Ag_{1.52}$	49.78	0.0044
AlAg[38]	10	$\alpha_{110} = -0.16$ $\alpha_{200} = 0.08$	$[Al–Al_{10.99}Ag_{1.01}]Al_{2.72}Ag_{0.28}$	7.86	0.2143
MgAg[38]	19	$\alpha_{110} = -0.13$ $\alpha_{200} = 0.26$	$[Ag–Ag_{9.42}Mg_{2.58}]Ag_{2.58}Mg_{0.42}$	18.74	0.0138
ZnAg[38]	50	$\alpha_{110} = -0.31$ $\alpha_{200} = 0.27$	$[Ag–Ag_{4.14}Zn_{7.86}]Ag_{1.90}Zn_{1.10}$	55.97	−0.1194
InMg[38]	12.5	$\alpha_{110} = -0.12$ $\alpha_{200} = 0.21$	$Mg–Mg_{10.32}In_{1.68}–Mg_{2.7}In_{0.3}$	12.35	0.0119
MoTi[38]	50	$\alpha_{110} = -0.29$ $\alpha_{200} = 0.04$	$Ti–Ti_{4.26}Mo_{7.74}–Ti_{1.56}Mo_{1.44}$	57.38	−0.1475
ReCo[38]	25	$\alpha_{110} = -0.11$ $\alpha_{200} = 0.18$	$Co–Co_{8.67}Re_{3.33}–Co_{2.39}Re_{0.61}$	24.66	0.0138
AlFe[38]	20	$\alpha_{110} = -0.14$ $\alpha_{200} = -0.07$	$Fe–Fe_{9.26}Al_{2.74}–Fe_{2.36}Al_{0.64}$	21.11	−0.0556

impedes ordered structure growth and promotes the formation of disordered solid solutions over long distances. The more homogeneous the alloy's microstructure is with fewer defects, the higher the performance it will exhibit. Therefore, various process treatments should be conducted during alloy smelting to enhance both the quantity and uniformity of solid solution clusters within the alloy.

5. Conclusions

In this study, we employed the FSPO of electron density for nearest-neighbor two-shell atoms to analyze the composition formula of FCC solid solution alloy. The key findings are as follows.

1. The analysis of the periodic oscillation distribution of electron density revealed that the central atom of the nearest-neighbor cluster should be situated in the second potential trough of FSPO, specifically at positions corresponding to the sixth, seventh, and eighth atomic shells. The associated vector sets are $< \pm1, \pm1, \pm1 >$, $< \pm3/2, \pm1, \pm1/2 >$, and $< \pm2, 0, 0 >$.
2. The analysis focused on the 1-3 cluster arrangement model, which complies with the FSPO in FCC solid solution alloys. The corresponding component structure formula is denoted as $[A–B_{12}]C_3$, where A represents the central atom, B denotes the first nearest-neighbor shell atom, and C signifies the second nearest-neighbor shell atom. This model exhibits a cluster coordination number of 14 and demonstrates the lowest relative mean deviation between the mean distance of the atoms on the cluster shell and the distance r_3 of FSPO. Furthermore, the model clusters demonstrate quadratic and hexagonal axisymmetric properties.
3. The Cowley parameters were employed to calculate the composition formula for two-shell atoms in various alloy configurations' nearest neighbors. The composition of this chemical structure formula was found to be largely consistent with that observed in actual alloys.
4. The analytical method and process proposed in this study can also be extended to other alloy systems, providing valuable theoretical support for developing new alloys and optimizing the properties of existing ones.

Acknowledgments

This work was supported in part by the Projects for the Department of Science and Technology of Fujian Province (Grant no. 2021-H-0060), the Natural Science Foundation of Sanming University (Grant no. 113/A160002), the Operational Funding of the Advanced Talents for Scientific Research (Grant no. 19YG04) of Sanming University, and the Fujian Province young and middle-aged teacher education research project (Grant no. JAT200624/B202015). The authors also acknowledge the support from the School of Mechanical and Electric Engineering, Sanming University.

References

1 R. Kurosawa, M. Takeuchi, and J. Ryu: RSC Adv. **11** (2021) 24292. https://doi.org/10.1039/D3RA05513B
2 E. Chan, J. Pásztorová, R. D. Johnson, M. Songvilay, R. A. Downie, J.-W. G. Bos, O. Fabelo, C. Ritter, K. Beauvois, Ch. Niedermayer, S.-W. Cheong, N. Qureshi, and C. Stock: Phys. Rev. B: Condens. Matter **106** (2022) 064403. https://doi.org/10.1103/PhysRevB.106.064403
3 A. Hussain, A. Kan, M. I. Khan, and S. U. Rehman: RSC Adv. **13** (2023) 29376. https://doi.org/10.1039/D3RA0551
4 Y. J. Zhang, D. Han, and X. W. Li: Scr. Mater. **178** (2020) 269. https://doi.org/10.1016/j.scriptamat.2019.11.049
5 D. Han, Y. J. Zhang, and X. W. Li: Acta Mater. **205** (2021) 116559. https://doi.org/10.1016/j.actamat.2020.116559
6 F. He, S. Wei, J. L. Cann, Z. Wang, J. Wang, and C. C. Tasan: Acta Mater. **220** (2021) 117314. https://doi.org/10.1016/j.actamat.2021.117314
7 S. Astafurov and E. Astafurova: Metals **11** (2021) 1052. https://doi.org/10.3390/met11071052

8 D. Vukelic, K. Simunovic, G. Simunovic, T. Saric, Z. Kanovic, I. Budak, and B. Agarski: J. Cleaner Prod. **266** (2020) 121919. https://doi.org/10.1016/j.jclepro.2020.121919
9 L. Jiang, B. Rouxel, T. Langan, and T. Dorin: Acta Mater. **206** (2021) 116634. https://doi.org/10.1016/j.actamat.2021.116634
10 L. Jiang, T. Langan, T. Wood, P. Sanders, and T. Dorin: Scr. Mater. **210** (2022) 114452. https://doi.org/10.1016/j.scriptamat.2021.114452
11 N. Kherrouba, B. Mehdi, R. Kouba, R. Badji, C. A. Dekik, and Y. T. Tounsi: Mater. Chem. Phys. **266** (2021) 124574. https://doi.org/10.1016/j.matchemphys.2021.124574
12 D. Han, X. J. Guan, Y. Yan, F. Shi, and X. W. Li: Mater. Sci. Eng., A **743** (2019) 745. https://doi.org/10.1016/j.msea.2018.11.103
13 R. Zhang, S. Zhao, J. Ding, Y. Chong, T. Jia, C. Ophus, M. Asta, R. O. Ritchie, and A. M. Minor: Nature **581** (2020) 283. https://doi.org/10.1038/s41586-020-2275-z
14 Z. Zhang, J. Wang, J. Qi, B. Wang, L. He, and D. Cang: Sci. China Ser. E: Technol. Sci. **38** (2008) 1050. https://doi.org/10.1360/ze2008-38-7-1050 (in Chinese).
15 O. V. Lushchikov, M. Gatchell, J. Reichegger, S. Kollotzek, F. Zappa, M. Mahmoodi-Darianc, and P. Scheier: Phys. Chem. Chem. Phys. **25** (2023) 8463. https://doi.org/10.1039/D2CP04569A
16 Q. Ma, H. Zhu, D. Liu, R. Li, T. Li, H. Ren, W. Zhao, Y. Pan, Y. Liu, and W. Guo: Catal. Sci. Technol. **13** (2023) 2080. https://doi.org/10.1039/D3CY00037K
17 D. A. Ryzhkova, S. L. Gafner, and Y. Y. Gafner: JETP Lett. **113** (2021) 638. https://doi.org/10.1134/S002136402110009XA
18 Q. Liu, P. Fan, Y. Hu, F. Wang, and L. Cheng: Phys. Chem. Chem. Phys. **23** (2021) 10946. https://doi.org/10.1039/D1CP00589H
19 W. Sun, Y. Zhu, R. Marceau, L. Wang, Q. Zhang, X. Gao, and C. Hutchinson: Science **363** (2019) 972. https://doi.org/10.1126/science.aav7086
20 Q. Zhang, Y. Zhu, X. Gao, Y. Wu, and C. Hutchinson: Nat. Commun. **11** (2020) 5198. https://doi.org/10.1038/s41467-020-19071-7
21 M. Zha, H. Zhang, H. Jia, Y. Gao, S. Jin, G. Sha, R. Bjørge, R. H. Mathiesen, H. J. Roven, H. Wang, and Y. Li: Int. J. Plast. **146** (2021) 103108. https://doi.org/10.1016/j.ijplas.2021.103108
22 H. H. Lu, H.-K. Guo, and W. Liang: Mater. Charact. **190** (2022) 112050. https://doi.org/10.1016/j.matchar.2022.112050
23 W. Mu, Y. Cai, and M. Wang: Mater. Sci. Eng., A **819** (2021) 141418. https://doi.org/10.1016/j.msea.2021.141418
24 Y. L. Qi, L. Zhao, X. Sun, H. X. Zong, X. D. Ding, F. Jiang, H. L. Zhang, Y. K. Wu, L. He, F. Liu, S. B. Jin, G. Sha, and J. Sun: J. Mater. Sci. Technol. **86** (2021) 271. https://doi.org/10.1016/j.jmst.2021.01.061
25 Y. H. Gao, L. F. Cao, J. Kuang, H. Song, G. Liu, J. Y. Zhang, and J. Sun: Mater. Sci. Eng., A **803** (2021) 140509. https://doi.org/10.1016/j.msea.2020.140509
26 S. Zhang, C. Dong, and P. Häussler: J. Vac. Sci. Technol., A **40** (2022) 022201. https://doi.org/10.1116/6.0001535
27 Z. Li, D. Dong, L. Zhang, S. Zhang, Q. Wang, and C. Dong: Sci. Rep. **12** (2022) 3169. https://doi.org/10.1038/s41598-022-06893-2
28 T. Mohri, D. D. Fontaine, and J. M. Sanchez: Metall. Trans. A **17** (1986) 189. https://doi.org/10.1007/BF02643894
29 Y. Honda, K. Tanaka, and T. Horiguchi: Phys. Rev. B: Condens. Matter **51** (1995) 15260. https://doi.org/10.1103/PhysRevB.51.15260
30 F. Walsh, M. Asta, and R. O. Ritchie: Proc. Natl. Acad. Sci. **118** (2021) e2020540118. https://doi.org/10.1073/pnas.202054011
31 P. Häussler: J. Phys. Colloques **46** (1985) 361. https://doi.org/10.1051/jphyscol:1985854
32 H. L. Hong, C. Dong, Q. Wang, Y. Zhang, and Y. X. Geng: Acta Physica Sinica **65** (2016) 036101. https://doi.org/10.7498/aps.65.036101
33 G. Grosso and G. P. Parravicini: Solid State Physics (Academic press, New York, 2013) Chap. 2.
34 P. Zhang, K. Shi, J. Bian, J. Zhang, Y. Peng, G. Liu, and A. Deschamps: Acta Mater. **207** (2021) 116682. https://doi.org/10.1016/j.actamat.2021.116682
35 Z. Z. Song, R. M. Niu, X. Y. Cui, E. V. Bobruk, M. Murashkin, N. A. Enikeev, R. Z. Valiev, S. P. Ringer, and X. Z. Liao: Scr. Mater. **210** (2022) 114423. https://doi.org/10.1016/j.scriptamat.2021.114423
36 J. M. Cowley: J. Appl. Phys. **21** (1950) 24. https://doi.org/10.1063/1.1699415
37 B. Schönfeld, L. Reinhard, G. Kostorz, and W. Bührer: Phys. Status Solidi B **148** (1988) 457. https://doi.org/10.1002/pssb.2221480203
38 V. I. Iveronova and A. A. Katsnel'Son: Soviet Phys. J. **19** (1976) 1002. https://doi.org/10.1007/BF00893800
39 T. Abbas and A. B. Ziya: J. Mater. Sci. **28** (1993) 5010. https://doi.org/10.1007/BF00361170